AD-A062 092 PURDUE UNIV LAFAYETTE IND PROJECT SQUID HEADQUARTERS F/G 20/4
THE GROWTH OF THE TWO DIMENSIONAL MIXING LAYER FROM A TURBULENT--ETC(U)
NOV 78 F K BROWAND, B O LATIGO N00014-75-1143
UNCLASSIFIED SQUID-USC-1-PU NL

| OF |
AD A062092

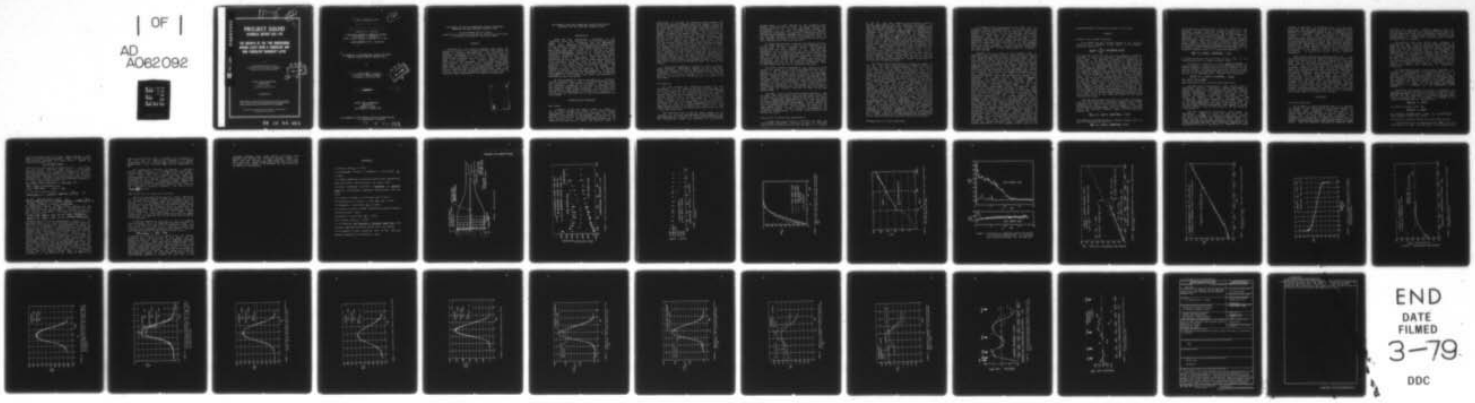

END
DATE FILMED
3-79
DDC

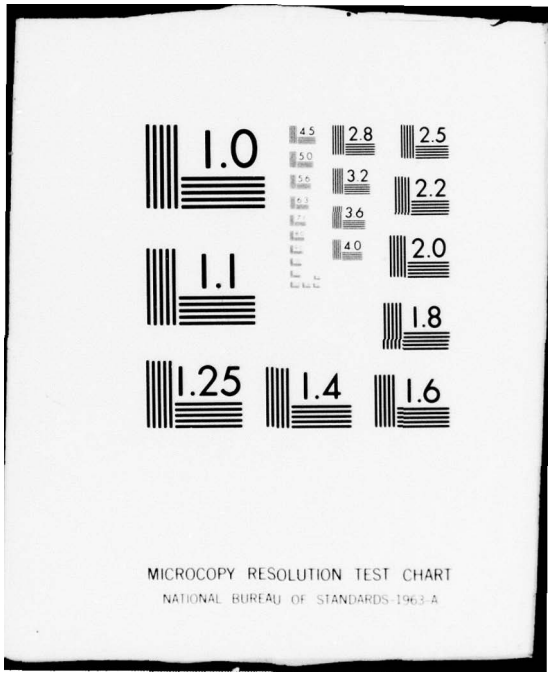
1.0
1.1
1.25
1.4
1.6
1.8
2.0
2.2
2.5
2.8
3.2
3.6
4.0
4.5
5.0
5.6
6.3
MICROCOPY RESOLUTION TEST CHART
NATIONAL BUREAU OF STANDARDS-1963-A

LEVEL II

12

SC

PROJECT SQUID

TECHNICAL REPORT USC-1-PU

THE GROWTH OF THE TWO DIMENSIONAL MIXING LAYER FROM A TURBULENT AND NON TURBULENT BOUNDARY LAYER

BY

F.K. BROWAND and B.O. LATIGO
UNIVERSITY OF SOUTHERN CALIFORNIA
LOS ANGELES, CALIFORNIA 90007

PROJECT SQUID HEADQUARTERS
CHAFFEE HALL
PURDUE UNIVERSITY
WEST LAFAYETTE, INDIANA 47907

NOVEMBER 1978

Project SQUID is a cooperative program of basic research relating to Jet Propulsion. It is sponsored by the Office of Naval Research and is administered by Purdue University through Contract N00014-75-C1143, NR-098-038.

(9) Technical Report USC-1-PU

(12)

(14) SQUID-USC-1-PU

PROJECT SQUID.

A COOPERATIVE PROGRAM OF FUNDAMENTAL RESEARCH
AS RELATED TO JET PROPULSION
OFFICE OF NAVAL RESEARCH, DEPARTMENT OF THE NAVY

CONTRACT N00014-75-1143 NR-098-038

(15)

(6) THE GROWTH OF THE TWO DIMENSIONAL MIXING LAYER FROM A TURBULENT AND NON TURBULENT BOUNDARY LAYER.

by

(10) F. K. Browand and B. O. Latigo
University of Southern California
Los Angeles, California 90007

(11) November 1978

(12) 39 p.

PROJECT SQUID HEADQUARTERS
CHAFFEE HALL
PURDUE UNIVERSITY
WEST LAFAYETTE, INDIANA 47907

403 617

THE GROWTH OF THE TWO DIMENSIONAL MIXING LAYER FROM A TURBULENT AND NON TURBULENT BOUNDARY LAYER

by F.K.Browand and B.O.Latigo
Department of Aerospace Engineering, University of Southern California, Los Angeles, California 90007

ABSTRACT

The effect of the initial boundary layer upon the downstream growth of the turbulent mixing layer between two streams is studied experimentally. Two conditions are carefully documented--in one case the boundary layers at separation are laminar; in the other case one boundary layer is made turbulent with a trip wire. When the boundary layer is turbulent, the lateral length scale, θ, characterizing the thickness of the mixing region, grows more slowly. At 400-500 initial momentum thicknesses downstream, the growth rate relaxes toward --but does not meet-- the growth rate of the untripped mixing layer. The lateral distributions of turbulence quantities, when scaled with the local lateral thickness, achieve the same form at distances beyond approximately 800 momentum thicknesses.

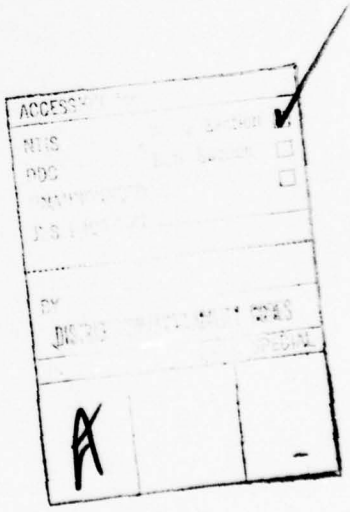

THE GROWTH OF THE TWO DIMENSIONAL MIXING LAYER FROM A TURBULENT AND NON TURBULENT BOUNDARY LAYER

INTRODUCTION

There has been considerable discussion in the literature about the sensitivity of the turbulent mixing layer, (c.f. Batt[1]; Champagne, Pao, and Wygnanski[2]; Foss[3]; Oster, Wygnanski, and Fiedler[4]). As a demonstration of this sensitivity, Brown and Roshko[5] gathered earlier data on mixing layer growth rates from a variety of sources. When these results were plotted as a function of speed ratio, $\lambda = (U_1 - U_2)/(U_1 + U_2)$, variations of as much as 30% were observed at intermediate values of λ, with even larger variations occurring near $\lambda = 1$. These variations may be attributed partly to experimental error and partly to differences in one or several of the conditions which define each experiment uniquely. Some of the more important variables which could affect the properties of the mixing layer are: the turbulence level of the free streams; the geometry of the test section, i.e., the distance and placement of walls; and the condition of the boundary layers at the point of mixing layer formation. It has also been suggested by Dimotakis and Brown[6] that the downstream development of the mixing layer itself can influence the upstream structure and growth.

We have attempted to isolate the effect of a different initial boundary layer upon the downstream mixing layer, while holding all other variables constant. Two conditions are carefully documented--in one case the boundary layers which form the mixing layer are laminar; in the other case one boundary layer is made turbulent. The only difference between the two experiments is the addition or removal of a trip wire on the high speed side of the plate separating the two streams.

APPARATUS AND PROCEDURES

Wind Tunnel

A schematic of the wind tunnel is shown in figure 1. Air is drawn through the tunnel by a blower located approximately 7 m from the plate trailing edge. The blower exhausts to the outside of the building. The 3x3 m stilling section is divided into two independent sections by a 10 cm deep splitter plate. Turbulence damping screens span the complete stilling section; while the splitter plate is

constructed in sections and carefully sealed against each screen with weather stripping, tape, and lacquer. (Some of our early operating problems were due to leakage from bottom to top around the screen seals.) Each box-like section of splitter plate contains an aluminum I-beam which is rigidly attached to the sides of the tunnel. This structure is needed to support the pressure difference (3-4 cm of water) between the top and bottom of the stilling section. The splitter plate tapers uniformly through the contraction section with an angle of two degrees. The final tapered section is a ground steel plate extending 46 cm into the test section and terminating with an edge thickness of about 0.5 mm. (The splitter plate taper occurs on the low speed side (upper side) only--the underside of the plate is flat and parallel to the bottom of the test section.) The tunnel is thus divided into two streams 30.5 cm deep and 91.4 cm wide. Unbleached cotton cloth is placed over the upper half of the entrance to the stilling section-- producing an increased pressure drop and hence a velocity difference at the plate trailing edge. For the cloth presently installed, the velocity ratio between the streams is about 5. --with a high speed stream velocity maximum of about 30 meters per second.

A probe drive mechanism is housed in a large, pressure tight plexiglass compartment resting on the tunnel roof. Probes are mounted on a vertical positioning drive, and are introduced through a hole in the tunnel roof into the low speed stream. A curtain attached to the vertical drive provides a false wall for the unused hole area ahead of the probe mount.

Flow Quality

The test section was carefully surveyed for flow uniformity. In the plane of the plate trailing edge, the flow is uniform across the cross section of the two streams to within $\pm .25\%$ of the maximum velocity. Wall boundary layers remain attached everywhere in the region of study. A typical boundary layer thickness on the bottom wall is 2.5 cm at x= 86 cm; while on the wind tunnel roof, the boundary layer thickness is of the order of 5 cm. The side wall boundary layers on the low speed side are of the order of 6 cm thick at x=86 cm. These measurements are for a high speed stream velocity of 26 meters per second and a low speed stream velocity of 5 meters per second, which is close to the test conditions.

The turbulence level in the low speed stream in the vicinity of the plate trailing edge is approximately 0.003 when expressed as a fraction of the velocity difference, ΔU. The fluctuations present are dominated by low frequency

acoustic noise. A broad maximum in the acoustic field extends from about 2 hz to 15 hz-- the blower rotation rate corresponds to 14 hz. In the high speed stream, the fluctuations are too small to be measured by our constant temperature anemometers. An equivalent turbulence level for the high speed stream(=0.0006ΔU), can be estimated by noting that the same (acoustic) pressure fluctuations are felt in both streams and produce velocity fluctuation levels which scale inversely with the velocity ratio.

At downstream stations, potential fluctuations are felt in the free stream as a result of the turbulence in the mixing layer and wall boundary layers. The potential fluctuations are first confined to the region near the boundaries, but as distance from the plate trailing edge increases, the fluctuations encompass a larger fraction of the free stream. At about x=86 cm, potential fluctuations from the top and bottom boundaries merge with fluctuations arising from the mixing layer. Beyond this point the fluctuation level in the free stream continually increases. At approximately x=220 cm, the rotational (turbulent) edges of the mixing layer and the top boundary layer meet.

The static pressures measured in the center of each stream are shown as a function of downstream distance in figure 2. The pressures are referenced to the static pressure in the low speed stream at the plate trailing edge, and are normalized by the dynamic pressure of the high speed stream. There is seen to be an initial acceleration in the high speed stream in the region near the plate trailing edge (=.009q in 15 cm), and thereafter a slight positive pressure gradient persists in both streams. This distribution of pressure is unaffected by the presence of the trip wire. The pressure difference across the mixing layer does seem to depend upon the velocity ratio, λ --at least in the high speed stream.

The small, positive downstream pressure gradient, .009q per meter, has little effect upon the high speed stream, but is reflected in a measurable deceleration of the low speed stream. Independent measurements of the stream velocities at various downstream positions (figure 3) are consistent with the pressure gradient measurements. Nominal values for the two stream velocities are 25.5 meters per second for the high speed stream, U_1 ; and 4.6 meters per second for the low speed stream, U_2. (When fluctuation measurements are normalized by $\Delta U = U_1 - U_2$, the actual local values at each station are used.)

Description of Mixing Layer Measurements

A single hot wire is used to determine the mean and fluctuating longitudinal velocity at each of 26 evenly spaced stations from the plate trailing edge to a distance

of 132 cm. The wire length is one millimeter, which is several times smaller than the turbulent microscale. At this farthest downstream station, the Reynolds number--based upon downstream distance and velocity difference--is 1.8×10^6; while the Reynolds number based upon maximum slope thickness (or vorticity thickness, δ_ω) is approximately 216,000. Expressed in multiples of the mixing layer vorticity thickness, the height of the tunnel is $4\delta_\omega$ and the breadth of the tunnel is $6\delta_\omega$ at x=132 cm. At each station, the hot wire is traversed slowly and continuously across the mixing layer, and the output recorded on FM magnetic tape. Travelling at a rate of approximately 0.25 millimeters per second, it takes between 10 and 20 minutes to complete each traverse. Beyond x=81.3 cm, the probe travel is not sufficient to completely span the mixing layer. In these cases two wires-- spaced approximately 10 cm apart in the vertical direction-- are used. Each profile thus consists of two segments recorded with different hot wires. In the central overlap region, slopes and values of the mean velocity are matched by making very slight corrections to the hot wire calibration curves.

The tape recorder bandwidth at 15 inches per second is 5000 hz. The top of the bandwidth is roughly a factor of 100 above the mean passage frequency of the vortex structures--very little energy is contained above this limit. The data are digitized (12 significant bits) at a fixed bandwith of 1000 hz. (This digitization bandwidth is unimportant if only means and rms values are required.) Means and rms fluctuations are defined by two second running sums. In two seconds the probe has travelled 0.5 mm which is insignificant compared to the thickness of the mixing layer. The averaging time typically corresponds to the passage time for 100 or more large scale vortical structures. Profiles of $\bar{u}(z)$ and urms(z) are plotted by computer. They do contain slight irregularities which are statistical fluctuations in the averages, but these are easily smoothed by eye. The single hot wire is sensitive to the total velocity in the plane normal to the wire, and thus responds to instantaneous values of v also. The correction to urms due to this effect is negligibly small (less than 1% of urms), and is therefore neglected. In addition to the measurements above, several measurements of the Reynolds stress, $\overline{u'v'}$, and of vrms, have been made using an x-wire probe. The sensing volume of the x-wire has the dimensions 0.25 mm by 0.38 mm by 0.5 mm. Calibration is performed by assuming a generalized polynomial form for the two instantaneous velocity components u and v in terms of the wire voltages. The ten required coefficients are determined by a least squares fit to approximately one thousand data points representing known velocities and flow directions.

Documentation of Initial Conditions

Two complete sets of measurements were made with two different initial boundary layers. In the first case, the boundary layers on both sides of the splitter plate were laminar at separation. In the second case, the boundary layer on the high speed side was tripped with a two dimensional wire (1.6 mm diameter), placed fifteen centimeters upstream from the plate trailing edge. (The equivalent flat plate Reynolds number at the plate trailing edge on the high speed side is about 10^6, so the boundary layer is easily tripped.) In terms of the displacement thickness of the undisturbed, laminar boundary layer, δ^*, the wire height is 1.6, and its position is 130 ahead of the trailing edge.

Evidence for the state of the boundary layer at separation was obtained from traverses across the flow at x=.25 mm downstream from the plate trailing edge. Figure 4(a) shows the mean velocity distributions on both sides of the plate with no trip, and on the low speed side with the trip in place (on the high speed side). These are compared with the circles representing the Blasius boundary layer. Momentum thickness on the high speed side is 0.457 mm without the trip, and 0.86 mm on the low speed side. Figure 4(b) gives the mean velocity on the high speed side with the trip in place. In this case, the momentum thickness is 0.81 mm. Representing the log region by the universal distribution gives a u_* value of 1.21 meters per second. This translates to a skin friction coefficient of 0.0015 at Re_θ=1350. The boundary layer is probably close to equilibrium, and the smallness of the wake region is consistent with a slightly accelerated flow at the plate trailing edge. The shape factor, δ^*/θ, is 1.42. The distributions of longitudinal velocity fluctuations, urms, across the boundary layers are shown in figure 5. Figure 5(a) gives the fluctuation distribution on the high speed side, tripped and untripped; and figure 5(b) gives the same data for the low speed side. The distribution of fluctuation amplitude in the tripped boundary layer is similar to the distribution in the turbulent flat plate boundary layer. However, the fluctuation amplitude remains at about 1% as the free stream is approached, and this is much higher than the previous values quoted for the free stream turbulence level. The reason is due to the noise introduced in the FM recording process, which is about .3% of the recorder dynamic range. Converting this noise to an equivalent velocity fluctuation roughly results in multiplication by a factor of four. Thus the 1% free stream turbulence level in the recorded signals is essentially all tape noise. It is the departures from this level which are most significant. In the laminar cases, these departures are small. The slight increases in fluctuation levels within the laminar boundary layer probably reflect the greater sensitivity of the boundary layer flow to the

unsteady pressure fluctuations present in the tunnel.

RESULTS

Growth of the Integral Thickness

The simplest and most reliable measure of the vertical extent of the turbulent mixing region is the integral thickness defined as:

$$\theta(\Delta U)^2 = \int_{-\infty}^{\infty} [U_1 - \bar{u}(z)][\bar{u}(z) - U_2]\, dz .$$

The length θ is here referred to as the momentum thickness although it does not represent a momentum defect in the usual sense. The momentum thickness is determined by integration of the mean velocity profiles at each of the 26 stations for the two cases. The results are shown plotted in figure 6 in non-dimensional form. The local momentum thickness and the downstream position are normalized by the initial momentum thickness. The initial momentum thickness for turbulent boundary layer is determined by extrapolating the measured momentum thickness values back to the origin x=0. This gives θ_i=.864 mm. For the laminar boundary layer, there are local departures from a strictly linear growth, and the initial momentum thickness is determined by an indirect method. A hot wire placed in the flow about 2 cm from the origin detects the initial unstable frequency in the laminar shear layer. Using linear stability theory, this frequency is related to the initial thickness of the shear layer at the point where the instability begins. The initial momentum thickness is determined to be θ_i=.46 mm. In both cases, the initial momentum thickness is very close to the value of the boundary layer momentum thickness on the high speed side, as one might anticipate for this large velocity ratio case.

The most interesting conclusion to be drawn from figure 6 is that the mixing layer grows more rapidly from a laminar boundary layer than from a turbulent boundary layer. The difference in growth rates is most apparant in the first 400-500 momentum thicknesses, where the momentum thickness growth for turbulent boundary layer is fit by the least squares line

$$\theta/\theta_i = [.0163 \pm .0002]\, x/\theta_i + 1.23.$$

The momentum thickness growth for laminar boundary layer is well fit everywhere by the line

$$\theta/\theta_i = [.0236 \pm .0008]\, x/\theta_i + 1.01 .$$

This difference in growth rate is not the result of the initially thicker turbulent boundary layer, for this dependence has been taken out by the normalization. If scale were the only difference, the two curves should be identical in this coordinate system. They are not identical--thus there is a fundamental difference between the two cases. (This result is also supported by numerous total pressure probe traverses which were recorded at an earlier date, but with one exception, are not shown here.) At 400-500 initial momentum thicknesses downstream, there is an abrupt increase in the growth rate (for the case of the turbulent boundary layer) to a value approximated by

$$\theta/\theta_i = [.0208 \pm .0006]\, x/\theta_i - .622.$$

It should be noticed that this slope is much closer to the slope obtained for the laminar boundary layer.

The physical location of the locus $\bar{u}(z) = (U_1 + U_2)/2$ is given in figure 7. Again both z and x are normalized by the initial momentum thickness, and z=0 is the location of the splitter plate. The normalized curves are little different for the two initial conditions except there seems to be more scatter in the untripped case. The best line is given by

$$z_o/\theta_i = [.0274 \pm .0003]\, x/\theta_i - 4.83,$$

for $500 < x/\theta_i < 2800$.

Mean Velocity Profiles and Fluctuation Amplitudes

The mean velocity distribution, when plotted with a normalized vertical coordinate, rapidly approaches an equilibrium shape. For both laminar and turbulent boundary layers, independence is established beyond 400 initial momentum thicknesses. Furthermore, the shape of the velocity distribution is identical in both cases. Figure 8 gives, as example, four mean distributions-- x/θ_i =1000,1780, for laminar separation; and x/θ_i =1000,1350, for turbulent separation. The four curves are so close as to be indistinguishable over most of the mixing layer. As the high speed stream is approached, there appears a slight velocity excess. This is often observed, and may indeed be a real effect.

The rms longitudinal fluctuation takes longer to equilibrate. Figure 9 gives the peak value of the fluctuation, urms/(ΔU), as a function of downstream distance for both the laminar and turbulent boundary layers. For laminar separation, the peak amplitude first rises to a value near 20%, and then approaches an equilibrium value of 16.7%$\pm$.5% beyond x/θ_i =400. For turbulent separation, the equilibrium value is approached at x/θ_i =800 by a steady

increase in amplitude. The variation with x of the peak values in the two cases is similar to the observations of Bradshaw[7] in the developing region of an axisymmetric jet. Contrary to Bradshaw's results however, the equilibrium values are identical within the estimated experimental accuracy. In fact, the distribution of fluctuation amplitude across the mixing layer is identical also. Figure 10(a) illustrates the nature of the equilibrium distribution by comparing profiles for laminar and turbulent boundary layers at two downstream locations, $x/\theta_i = 1780$ and $x/\theta_i = 1000$, respectively. These results are typical of all the profiles in the equilibrium region. Figure 10(b) illustrates the differences in the profiles in the region preceeding equilibrium. An equilibrium profile is also shown for comparison.

More recently, properties involving both u and v have been measured at x=81 cm. Again the only difference is the presence or absence of the trip wire attached to the high speed side of the plate, but the value of λ is slightly higher than for the previous measurements --0.82 as opposed to 0.69. With the trip wire in, the physical momentum thickness is smaller by about 25%; yet the distributions of means and fluctuations are very close indeed. The present data were obtained with an x-wire probe, and utilize a calibration procedure quite different from the earlier, single wire results. Figures 11, 12, and 13 give the distributions of urms, vrms, and $\overline{u'v'}$ respectively for the two boundary layer conditions. The results for urms, tripped and untripped, are indistinguishable from one another and agree well with the distributions recorded earlier. The distributions of vrms are virtually identical also--with a peak value just slightly under 13.%. The largest difference between the two cases occurs in the peak value of the Reynolds stress, figure 13, but this difference is the same order as the scatter in the data.

DISCUSSION

Universal Similarity

On the basis of results presented here, it is possible to conclude that the distributions of both mean velocity and the second order turbulence quantities achieve an equilibrium state independent of the condition of the initial boundary layer, provided the lateral coordinate is scaled with the local mixing layer thickness. This independence is established for second order quantities at a distance of about 800 initial momentum thicknesses from the origin. These distributions could depend upon the speed ratio; thus they represent a possible one parameter family

with λ as the parameter. Evidence suggests that the distribution of mean velocity, when plotted as in figure 8, is very insensitive to λ and is universally applicable. The distributions of second order turbulence quantities may depend upon λ (c.f. Yule[8], Batt[9]), but more data is needed to define this relationship.

The growth of the local mixing layer thickness is different by about 12% for the two cases considered. As shown earlier, with turbulent boundary layer the mixing layer at first grows more slowly-- then relaxes toward the growth rate of the untripped layer. The relaxation is significant, but to say the mixing layer growth rate achieves complete independence from conditions at formation is probably not justified. (Taking into account the possible errors, the growth rates still differ by about 6%.) We have no ready exlanation for the differences in growth rate which persist downstream of the relaxation. It is, however, a dramatic illustration of the sensitivity of mixing layer growth upon variations in experimental conditions.

The advantage of using a local lateral length, θ, for scaling the distributions of properties--rather than a coordinate proportional to $1/(x-x_o)$--is now clear. A scaling with distance from the origin (or effective origin) must implicitly include the growth rate of the mixing layer. The existence of different growth rates among various experiments-- even those at constant λ --probably explains the scatter in some of the published experimental comparisons (c.f. Champagne, Pao, and Wygnanski[2], Batt[9], Patel[10]).

The mixing layer growth rate will be different for different values of the velocity ratio, λ. Using the result $\delta_\omega = 5\theta$ (where δ_ω is the vorticity thickness), and the value $\lambda = .695$ for our experiment, a vorticity thickness growth rate can be established. If the growth is assumed to be linearly dependent upon λ, the result is

$$d\delta_\omega/dx = .170\lambda$$

for laminar boundary layer, and

$$d\delta_\omega/dx = .150\lambda$$

for turbulent boundary layer. Brown and Roshko[5] suggest a value between 0.162λ and 0.181λ.

Calculation of Reynolds Stress and Lateral Mean Velocity

The calculation of the Reynolds stress, $\overline{u'v'}$, from the distribution of mean velocity, $\bar{u}(z)$, is a procedure which

relies upon similarity of the flow. This technique is often used as a check on the measurement of $\overline{u'v'}$. We have applied the following procedure with good results. Assume the similarity variable to be

$$\eta = (z - z_0(x)) / \theta(x) ,$$

where $z_0(x)$ is the location of $\bar{u}(z)=(U_1+U_2)/2$. (z_0 is chosen for the lateral reference point since it is an easily measured quantity, c.f. Townsend[11], Liepmann and Laufer[12].) Both $z_0(x)$ and $\theta(x)$ are assumed to be linear functions of x. (The x momentum equation will be used without the pressure gradient term. The small, positive pressure gradient in the experiment can be shown to contribute negligibly compared to the other terms in the equation.) Let

$$f(\eta) = [\bar{u}(z) - (U_1+U_2)/2]/(U_1-U_2)/2 = \bar{u}(z)/\Delta U/2 - 1/\lambda ,$$

$$h(\eta) = [\bar{v}(z) - (V_1+V_2)/2]/(V_1-V_2/2 ,$$

$$g(\eta) = \overline{u'v'}/(\Delta U)^2 , \qquad F(\eta) = 1 - f(\eta) .$$

The continuity equation gives

$$(\Delta V/\Delta U)(h(\eta)-1) = -(dz_0/dx)F - d\theta/dx\left[\eta F - \int_{-\infty}^{\eta} F d\eta\right], \qquad (1)$$

and the x momentum equation gives

$$g(\eta) = 1/4\, d\theta/dx\left[(1+1/\lambda)FA - F\left(\int_{-\infty}^{\infty} F d\eta - \tfrac{1}{2}\int_{-\infty}^{\infty} F^2 d\eta\right) - (1+1/\lambda)\left(\eta F - \int_{-\infty}^{\eta} F d\eta\right)\right. \qquad (2)$$
$$\left. + F\int_{-\infty}^{\eta} F d\eta - \int_{-\infty}^{\eta} F^2 d\eta\right], \quad A = \lim_{\eta\to\infty}\left(\eta - 1/2\int_{-\infty}^{\eta} F d\eta\right).$$

By integrating to $\eta=+\infty$, two equations are produced for the four unknowns V_1, V_2, dz_0/dx, $d\theta/dx$. The equations are used with specified $f(\eta)$, dz_0/dx, $d\theta/dx$ to determine V_1, V_2 --the mean lateral velocities at the edges of the mixing layer. For the conditions

$dz_0/dx = .032$, $d\theta/dx = .0278$, $\lambda = .82$, laminar boundary layer;

$dz_0/dx = .032$, $d\theta/dx = .0242$, $\lambda = .81$, turbulent boundary layer;

corresponding to the recent measurements (figure 13), the momentum equation is then integrated as a function of η. The results are compared with the measurements in figure 14. There is a difference of 20% between the calculated and measured peak values of the Reynolds stress for the laminar boundary layer, and about a 10% difference for the turbulent boundary layer. The computation is very sensitive to the choice of the mixing layer growth rate. In both cases, the growth rates used are linear extrapolations in λ from the careful measurements at $\lambda = .695$, and should be accurate within ±6%--accounting also for uncertainty in λ. The experimental values could be revised upward by several per cent (a correction for the limited bandwith used). For the laminar case this accounts for only half of the difference, and it is difficult to say whether the calculation or the measurement is the more reliable result. It is interesting to note that the computed shape, $g(\eta)$, is practically independent of the speed ratio, λ. When the shape of the

mean velocity profile, $F(\eta)$, is assumed to be independent of λ, the term in brackets in equation 2 is nearly proportional to $1/\lambda$. Thus if $d\theta/dx$ is taken to be linearly proportional to λ, the shape, $g(\eta)$, will be independent of λ.

The computation procedure anticipates a non-zero lateral mean velocity on both sides of the mixing layer. For the laminar boundary layer, $V_1/\Delta U = +.015$, and $V_2/\Delta U = -.017$; while for the turbulent boundary layer the corresponding values are +.023 and -.009. The calculated distributions are compared with the measured lateral mean velocities in figure 15. The agreement is good considering the difficulty in making a reliable measurement of $\bar{v}(z)$. In particular, the point of maximum velocity is well matched. The continuity equation predicts this point to be $\eta_{\bar{v}_{max}} = -\frac{dz_0/dx}{d\theta/dx} \approx -1.0$.

Implications for the Large Scale Structure

While the preceding results give no direct indication of the presence or absense of large scale structure, there are several implications. When the boundary layer is laminar, let it be assumed that the mixing layer grows by the interaction and pairing of the now familiar large scale structures. When the boundary layer is turbulent, the mixing layer growth rate is initially much smaller, and it is reasonable to conclude that the introduction of small scale turbulence has obstructed the large scale interactions. In the eventual relaxation toward the higher growth rate, the important role of the large scale structure is reestablished.

As partial support for this idea, it can be observed that the growth rate of the momentum thickness (figure 6) is fit by a straight line, but there are departures from this line which do not seem to be completely random. The residual local thickness, defined as the difference between the measured momentum thickness and the best line fit

$$(\theta/\theta_i)_{residual} = \theta/\theta_i - \bar{\theta}/\theta_i ,$$

is plotted as a function of x in figure 16 for the laminar boundary layer. Also plotted on this figure are the downstream positions where the local momentum thickness doubles in value. These positions of doubling seem to be correlated with regions of large local growth rate. One possible explanation is that the pairing interactions which produce mixing layer growth are more likely to occur at certain downstream positions. These are the positions of most rapid growth rate--and they are spaced at intervals corresponding roughly to a doubling in thickness. If the same residual thickness is plotted for the case of the

turbulent boundary layer, much smaller deviations from straight line growth are initially evident, figure 17. Again this may indicate an some inhibition of the large scale structure. Farther downstream larger local variations in growth rate begin to be observed, but the results are scattered and inconclusive.

REFERENCES

1 R.G.Batt, AIAA 13, 2 (1975).

2 F.H.Champagne, Y.H.Pao, I.J.Wygnanski, J. Fluid Mech. 74, 2 (1976).

3 J.F.Foss, Symposium on Turbulent Shear Flows, Pennsylvania State University, University Park, Pa. (April 1977).

4 D.Oster, I.Wygnanski, H.Fiedler, Turbulence in Internal Flows, ed. S.N.B.Murthy, (Hemisphere Publications, 1976), pp 67-87.

5 G.L.Brown, A.Roshko, J. Fluid Mech. 64, 4 (1974).

6 P.E.Dimotakis, G.L.Brown, J. Fluid Mech. 78 3 (1976).

7 P.Bradshaw, J. Fluid Mech. 26, 2 (1966).

8 A.J.Yule, R. and M. no.3683 (Aeronautical Research Council of Great Britain, 1972).

9 R.G.Batt, J. Fluid Mech. 82, 1 (1977).

10 R.J.Patel, AIAA 11, 1 (1973).

11 A.A.Townsend, The Structure of Turbulent Shear Flow, (2nd edition, Cambridge University Press, 1976), pp 195-205.

12 H.Liepmann, J.Laufer, Technical Note no.1257 (National Advisory Committee for Aeronautics, 1947).

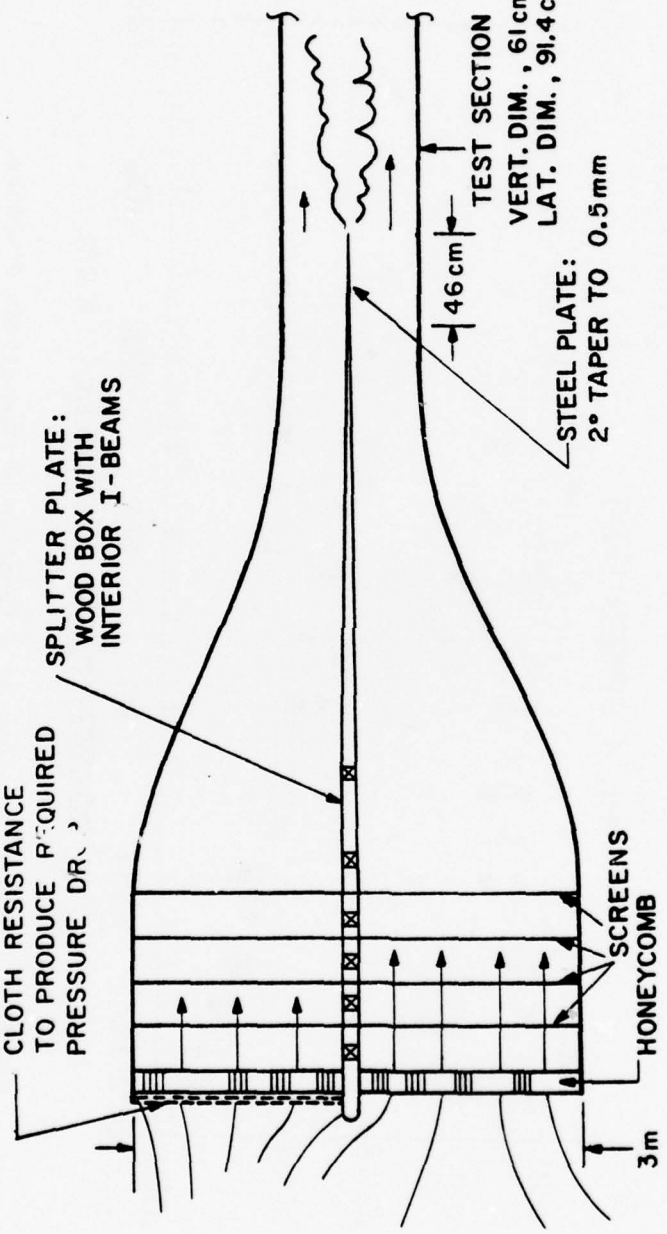

FIGURE 1. Sketch of wind tunnel.

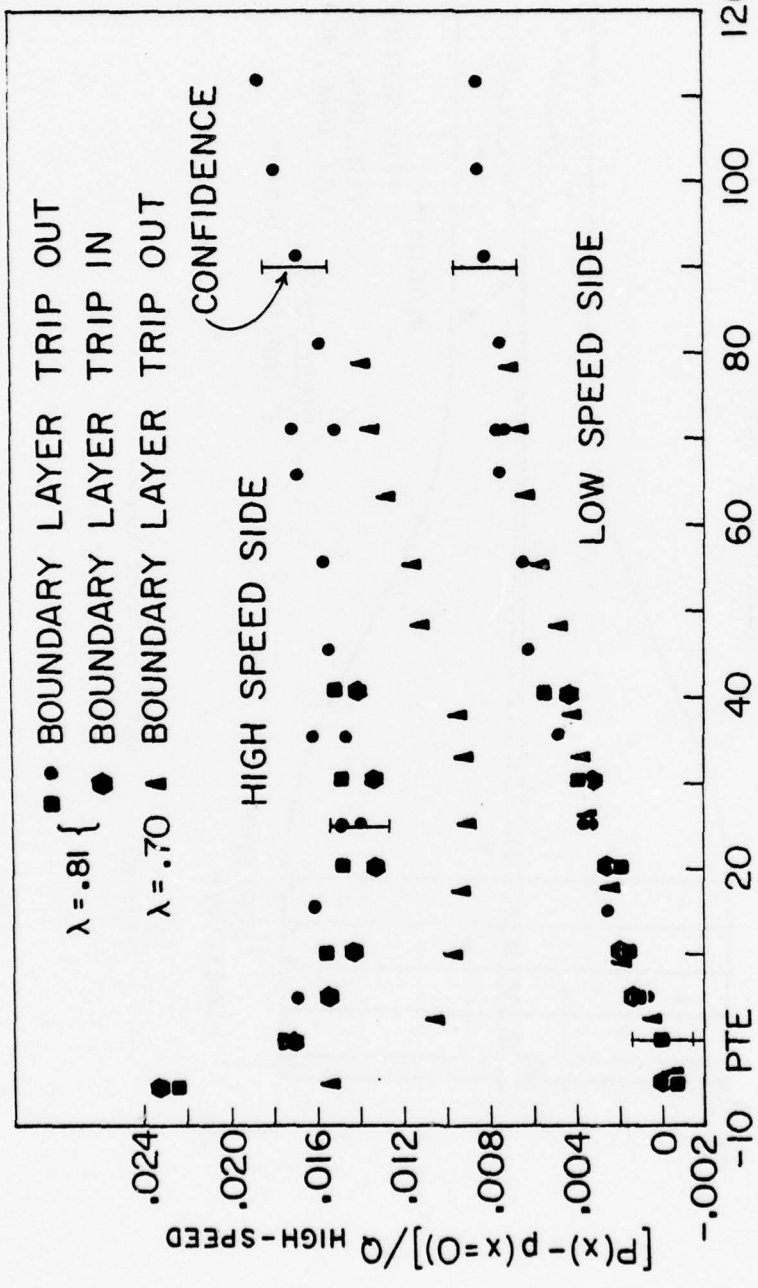

FIGURE 2. Static pressure as a function of downstream distance.

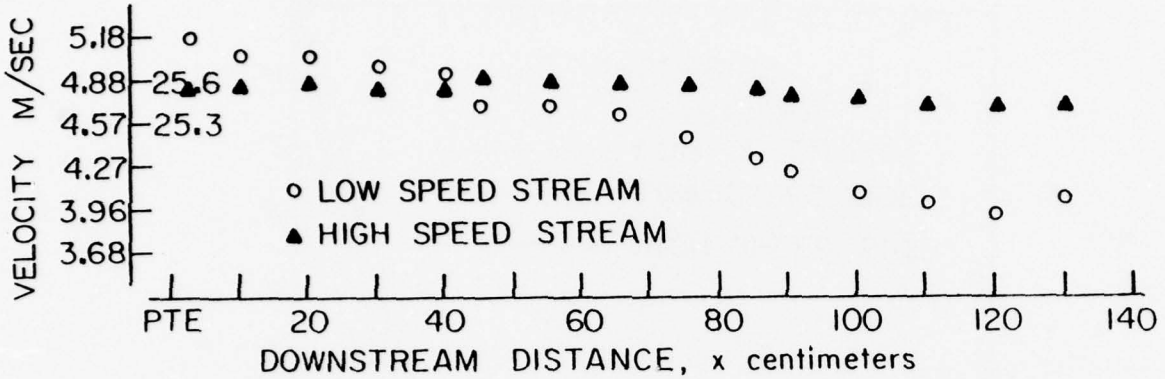

FIGURE 3. Free stream velocities as a function of downstream distance.

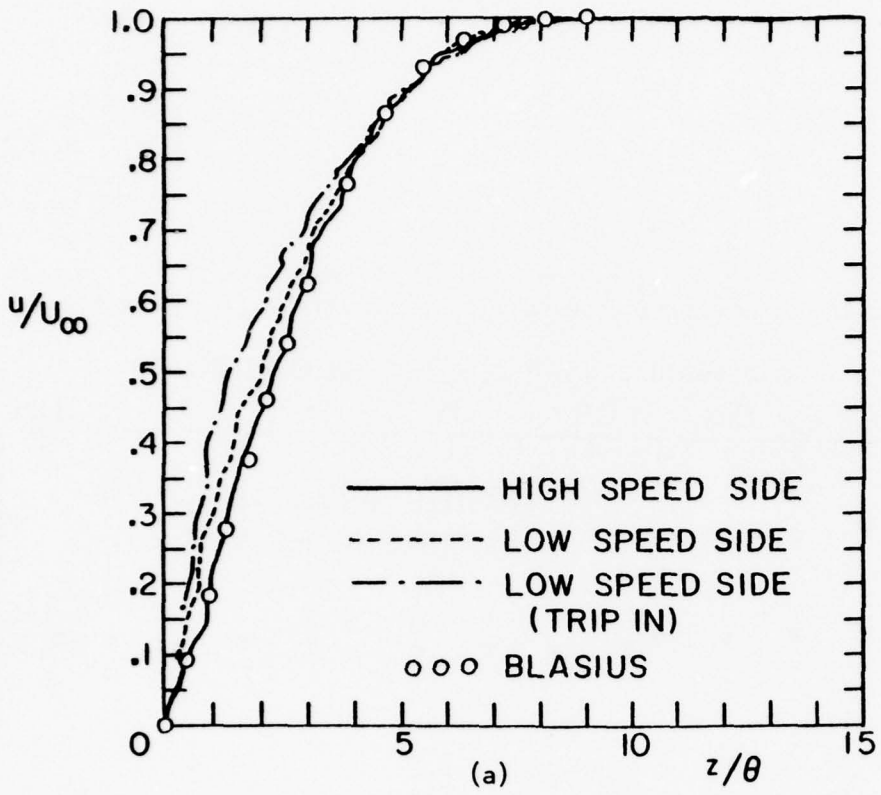

FIGURE 4. Mean velocity distributions in splitter plate boundary layers. (a) High speed side untripped, and low speed side.

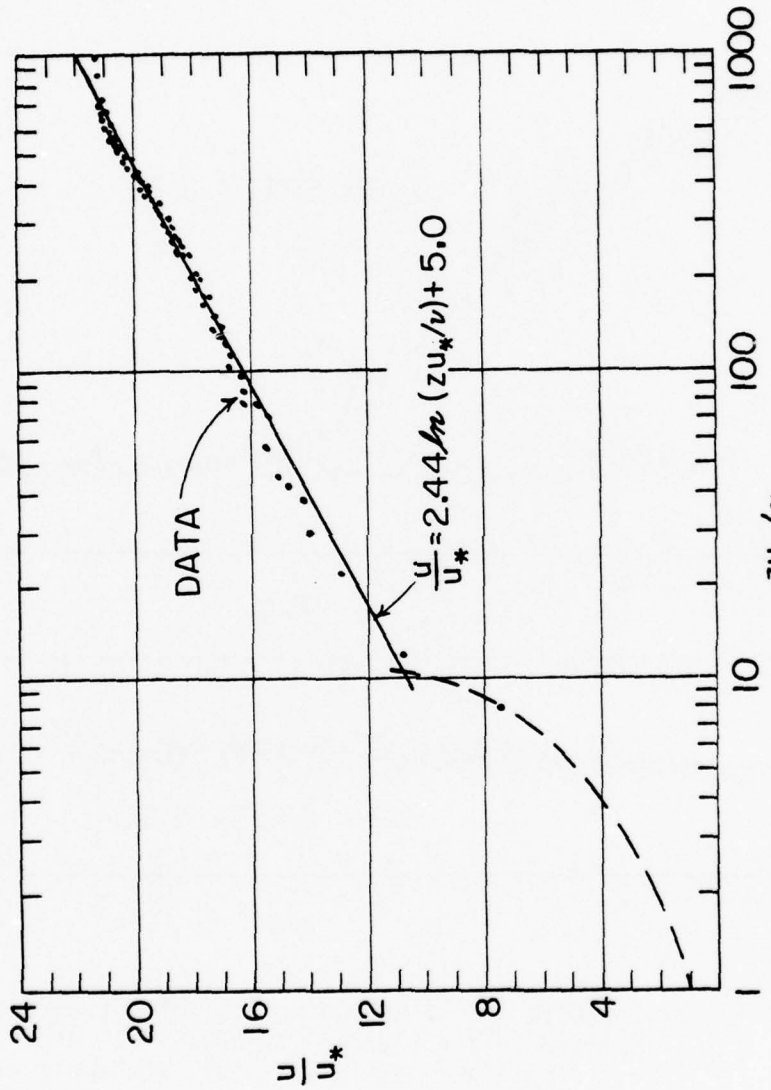

FIGURE 4. Mean velocity distributions in splitter plate boundary layers.
(b) High speed side tripped.

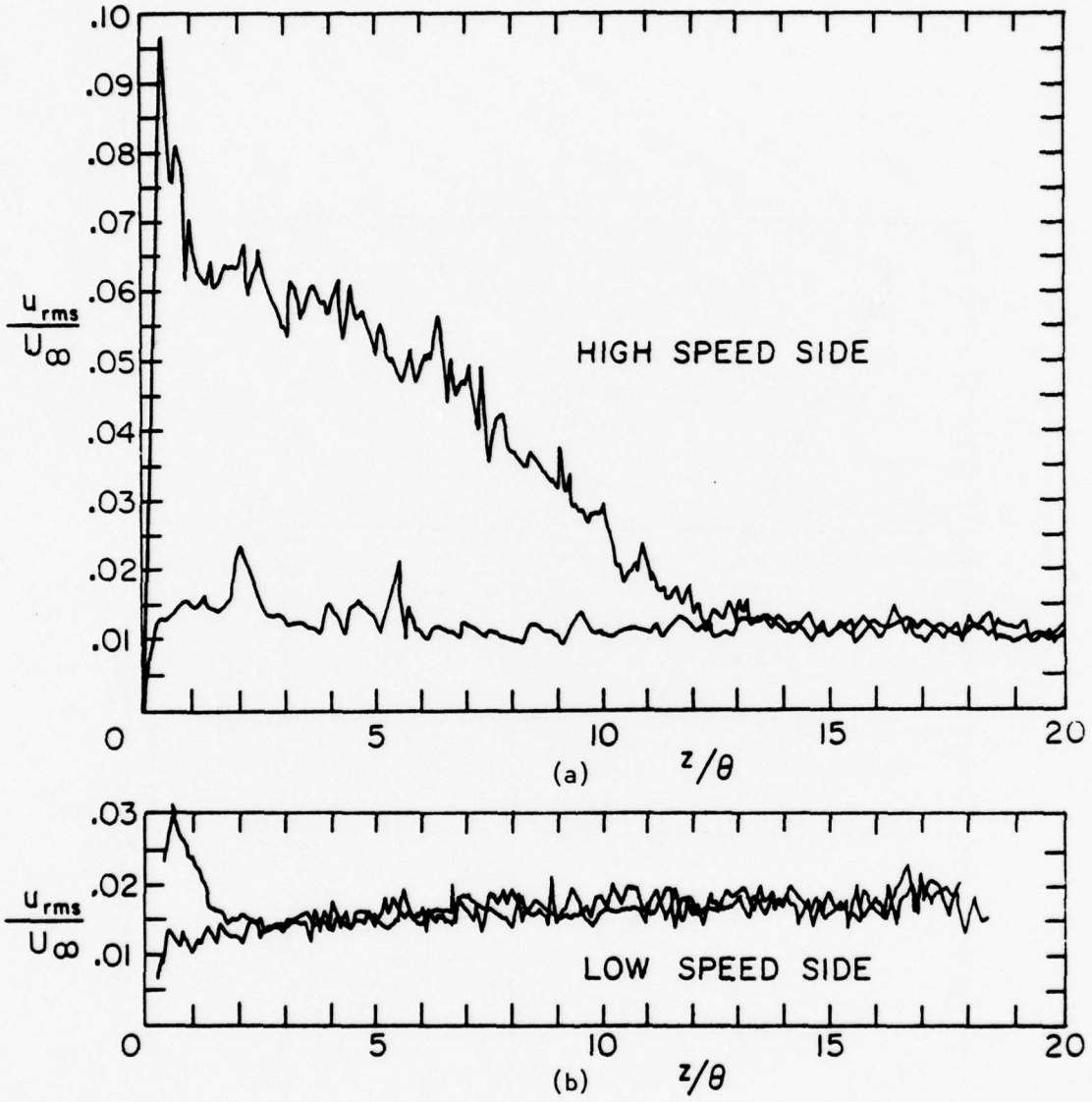

FIGURE 5. Distributions of longitudinal velocity fluctuations in splitter plate boundary layers. (a) High speed side, tripped and untripped; (b) Low speed side.

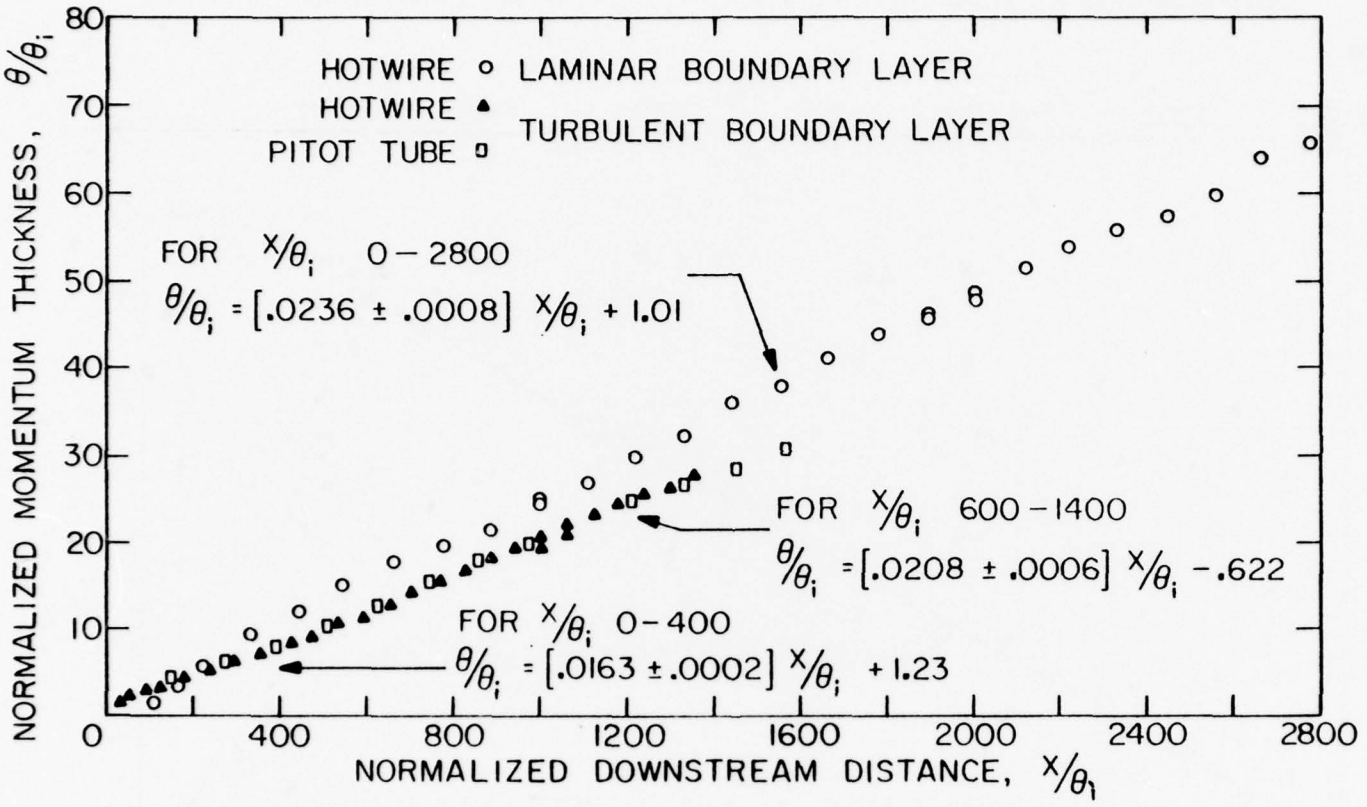

FIGURE 6. Normalized local momentum thickness as a function of downstream distance for $\lambda = .695$.

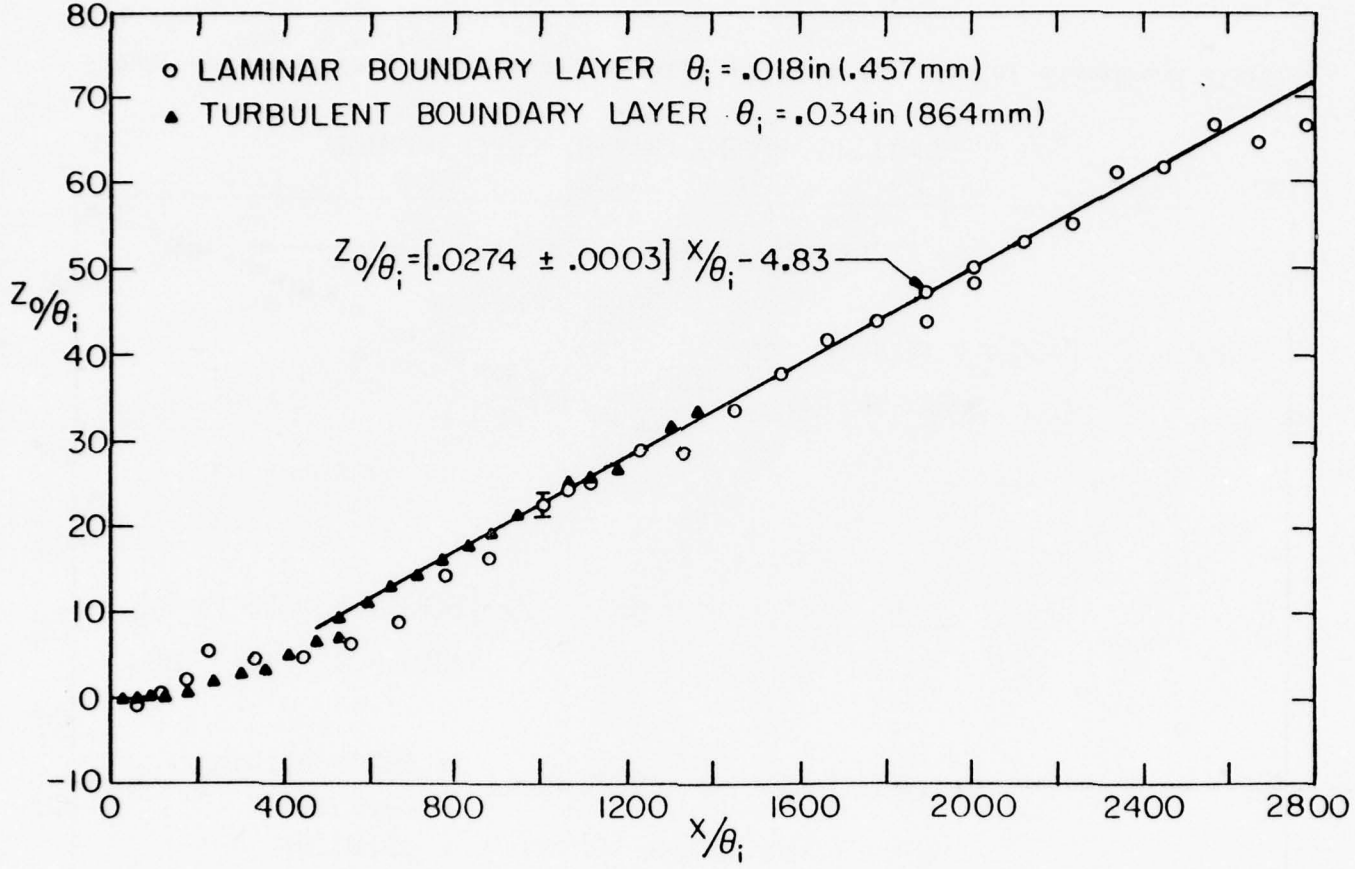

FIGURE 7. Position of the point, z, where $\bar{u}(z) = (U_1 + U_2)/2$ versus downstream distance for λ = .695.

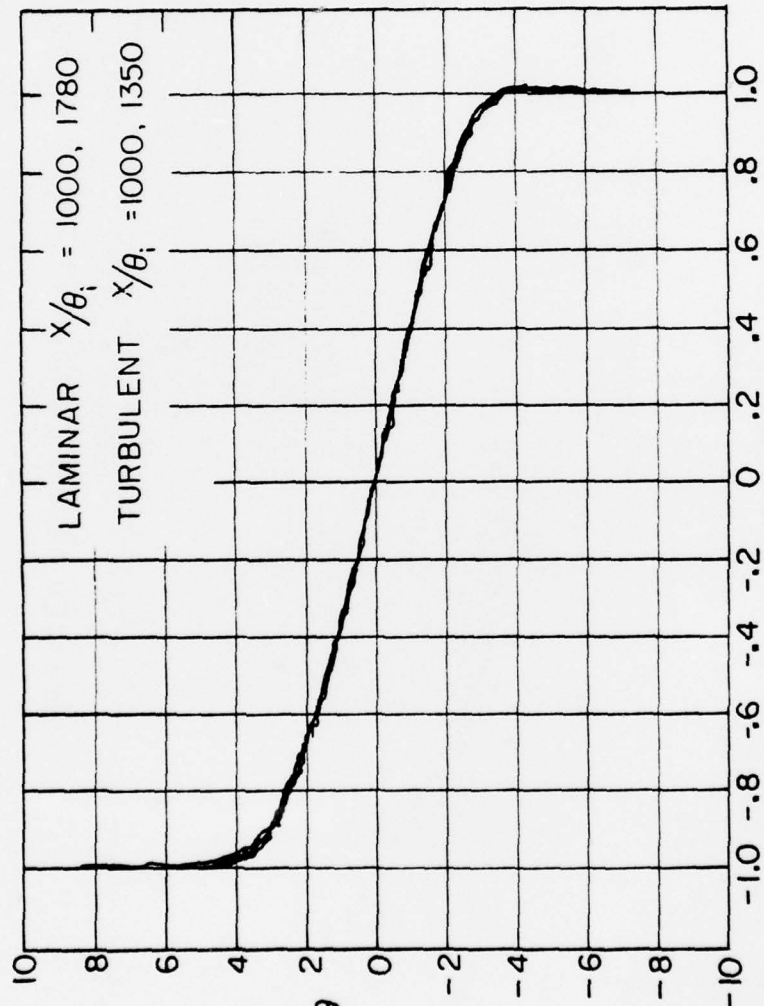

FIGURE 8. Profiles of longitudinal mean velocity at various downstream stations. (The point $z=z_o$ is the origin of the lateral scale.)

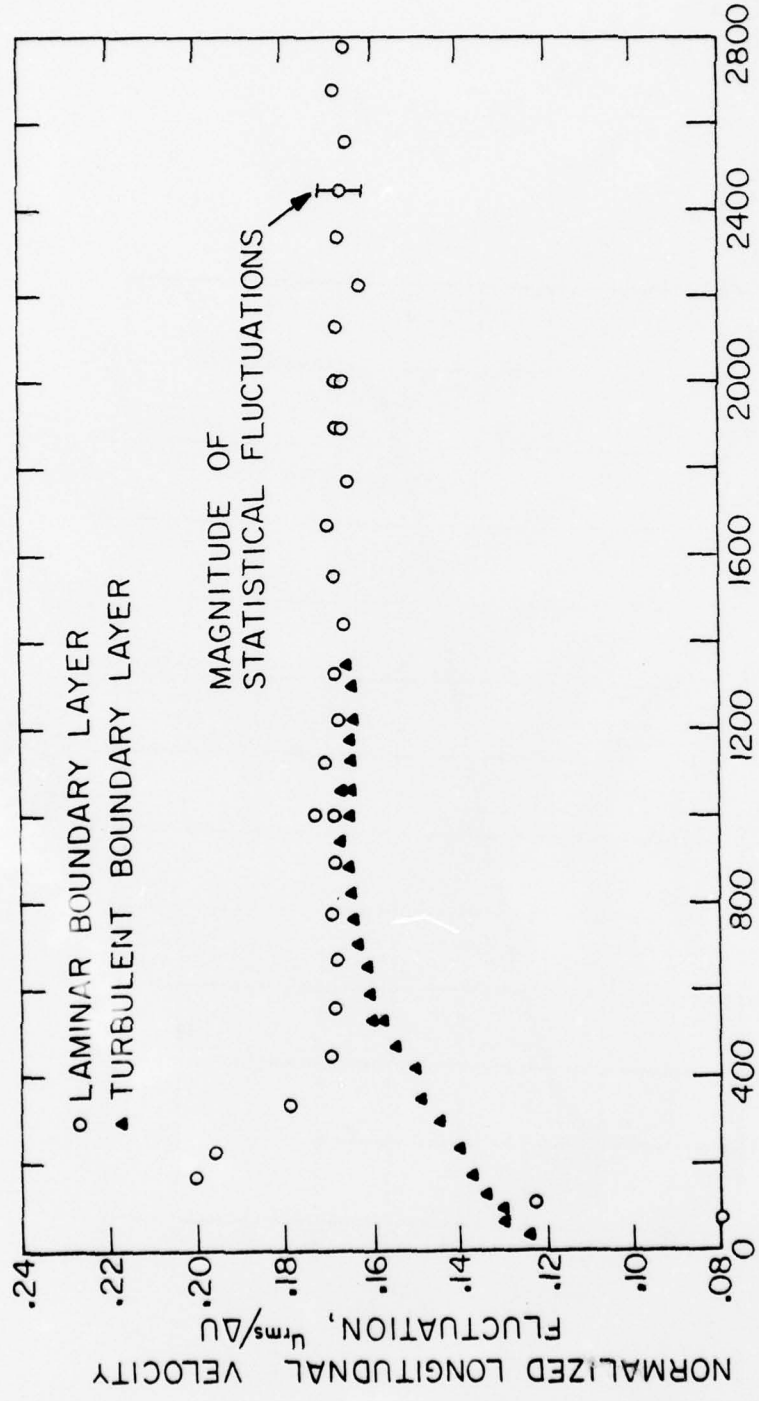

FIGURE 9. Peak values of the longitudinal velocity fluctuation as a function of downstream distance.

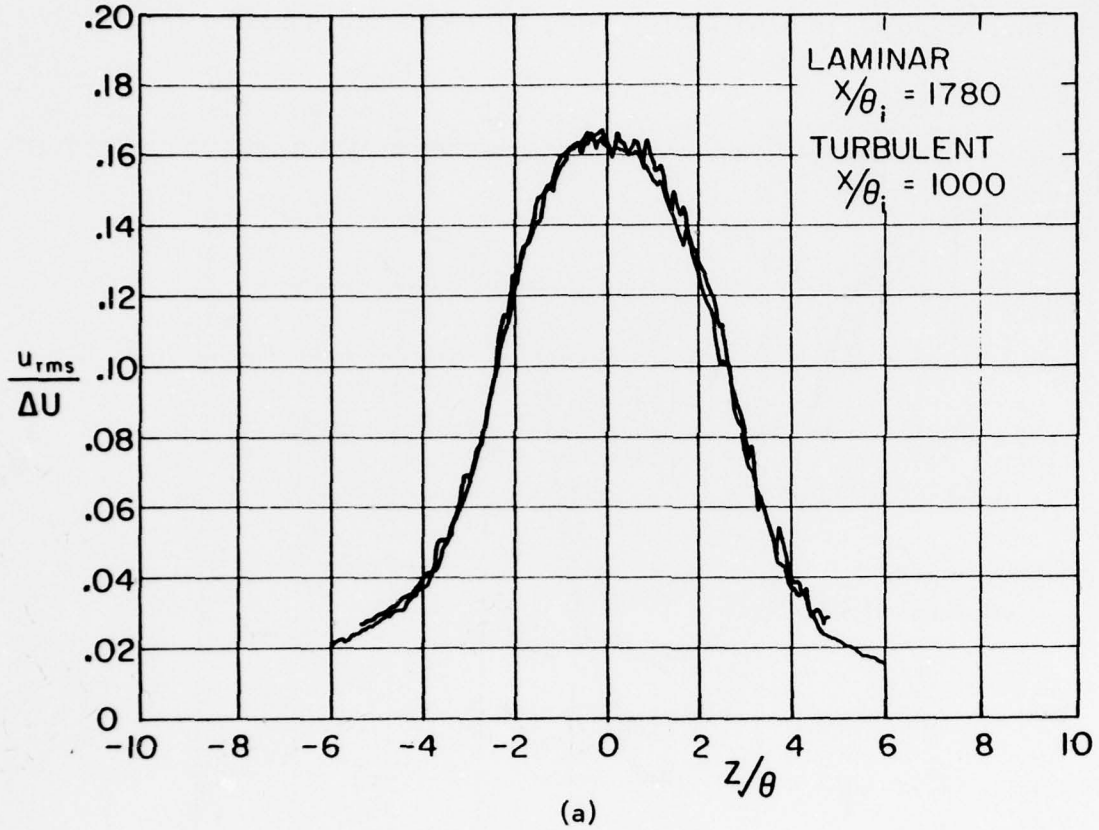

(a)

FIGURE 10. Distributions of longitudinal velocity fluctuation at various downstream stations for $\lambda = .695$. (Origin for lateral scale is $z = z_o$.) (a) The equilibrium distribution.

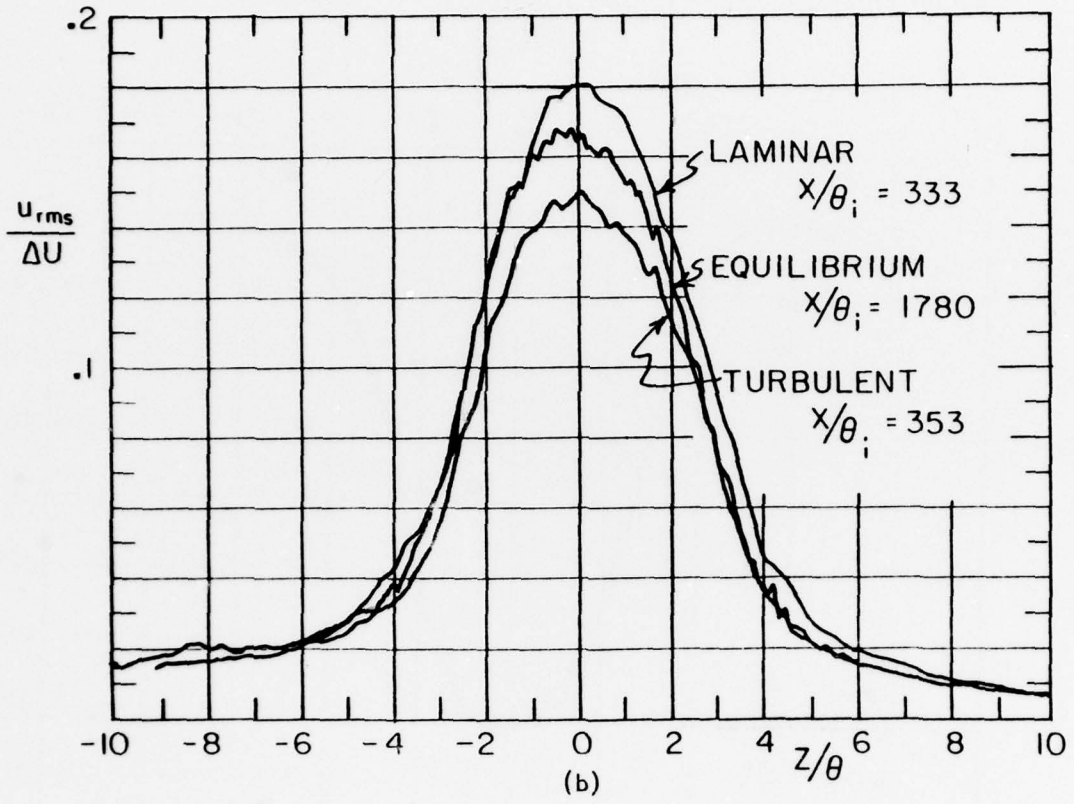

FIGURE 10. Distributions of longitudinal velocity fluctuation at various downstream stations for λ =.695. (Origin for lateral scale is $z = z_o$.) (b) Differences preceding equilibrium.

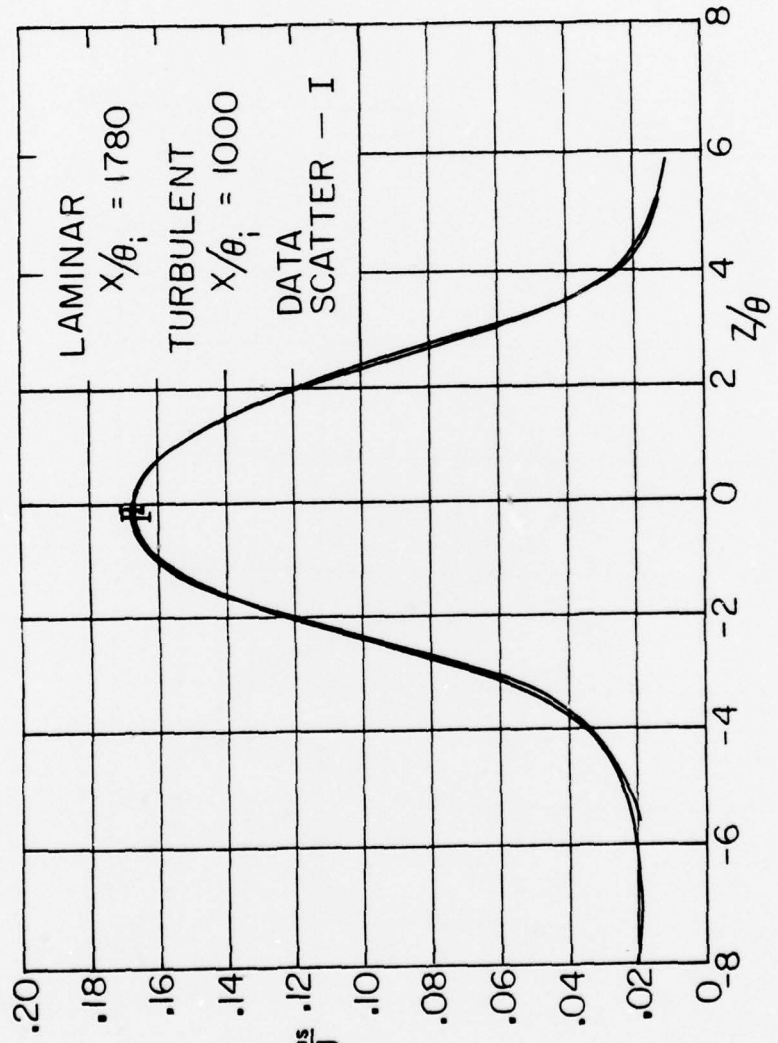

FIGURE 11. Distributions of longitudinal velocity fluctuation for $\lambda \approx .82$. (Origin for lateral scale is $z=z_o$.)

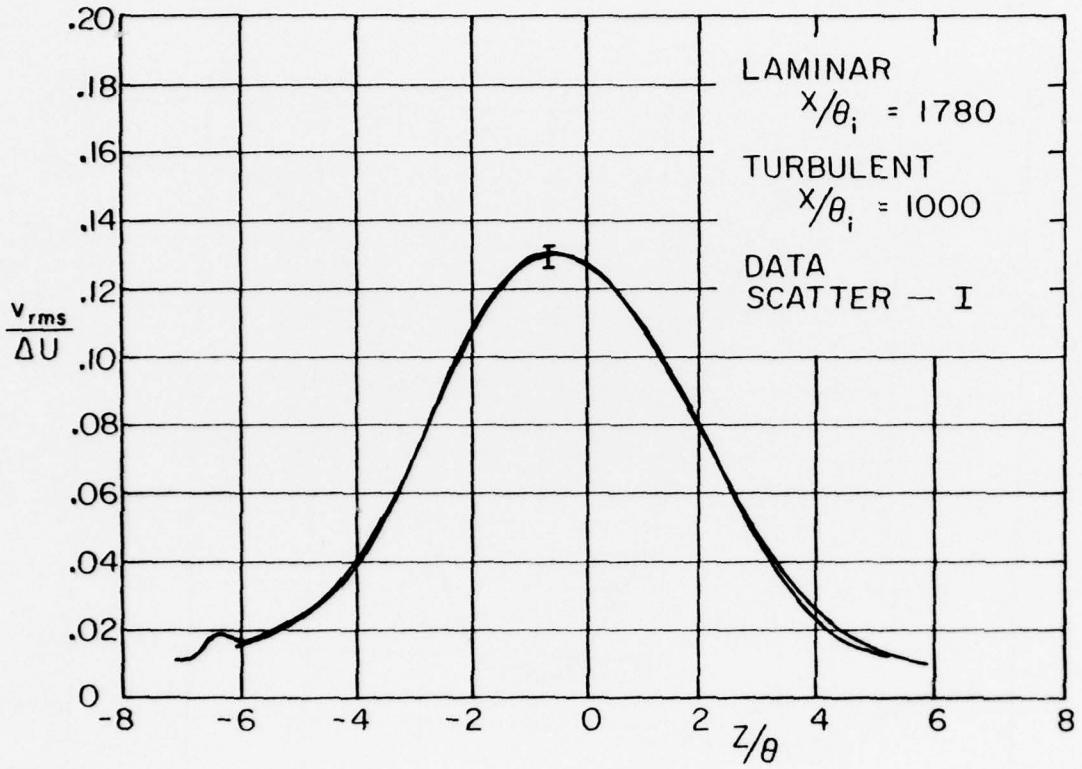

FIGURE 12. Distributions of lateral velocity fluctuation for $\lambda \approx .82$.

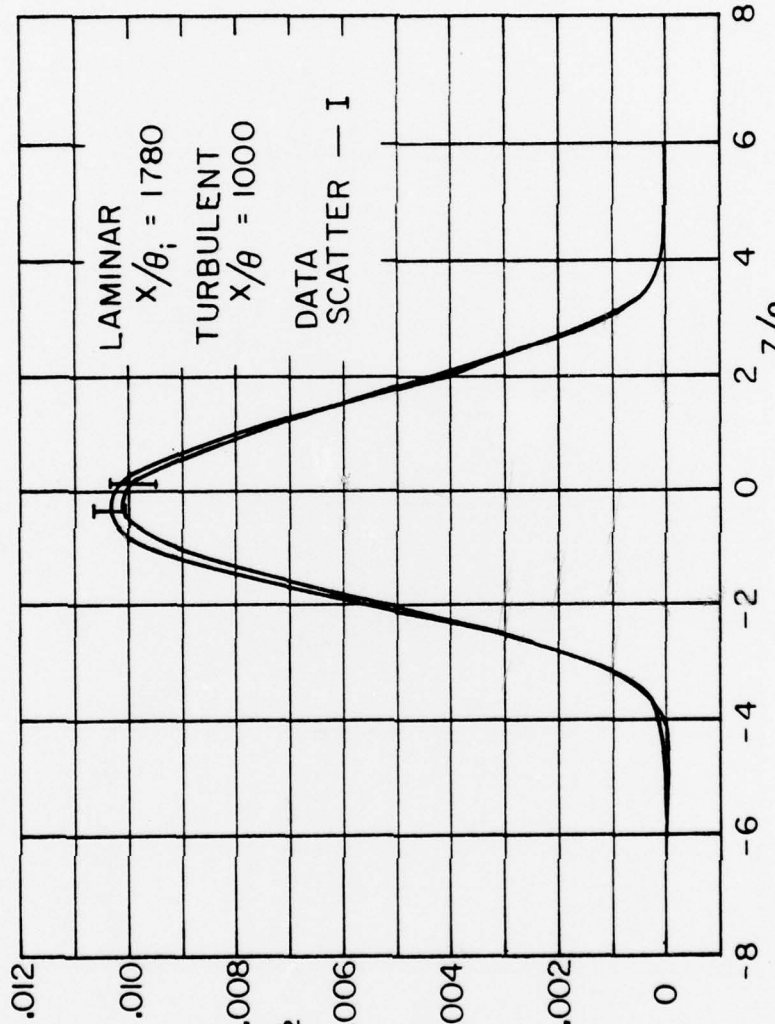

FIGURE 13. Distributions of Reynolds stress for $\lambda \approx .82$.

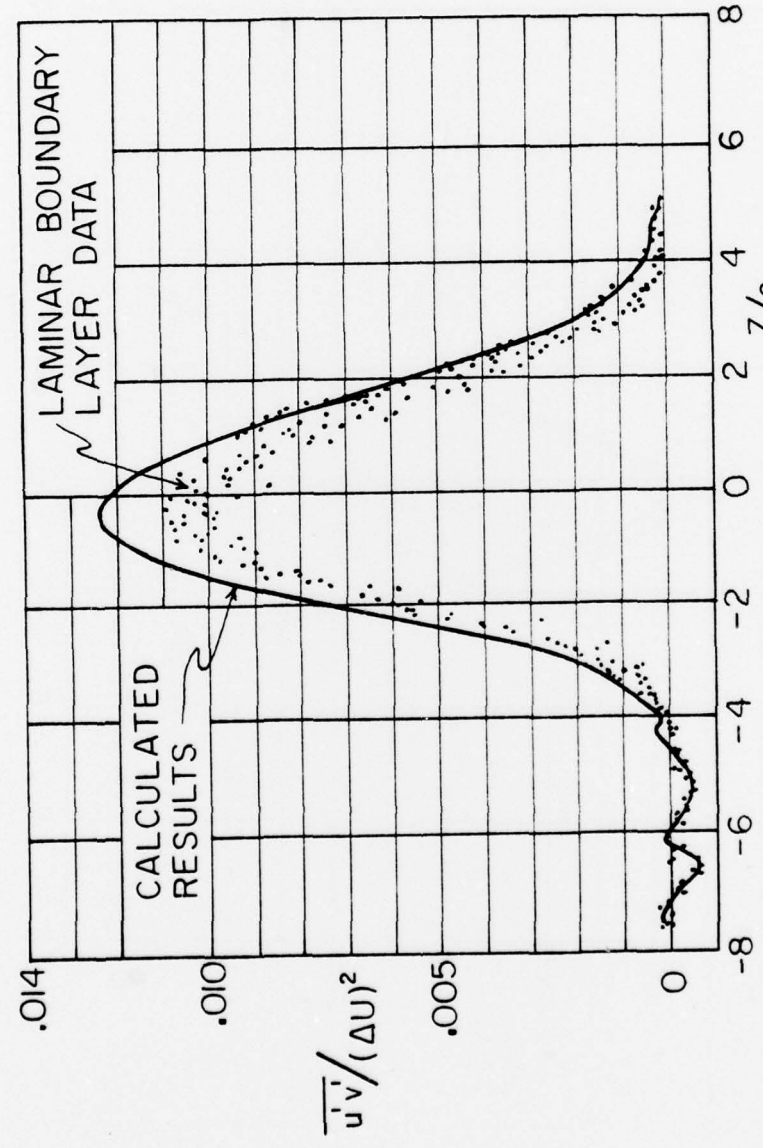

FIGURE 14. Comparison of computed and measured Reynolds stress distributions, (a) Laminar boundary layer, $\lambda = .82$.

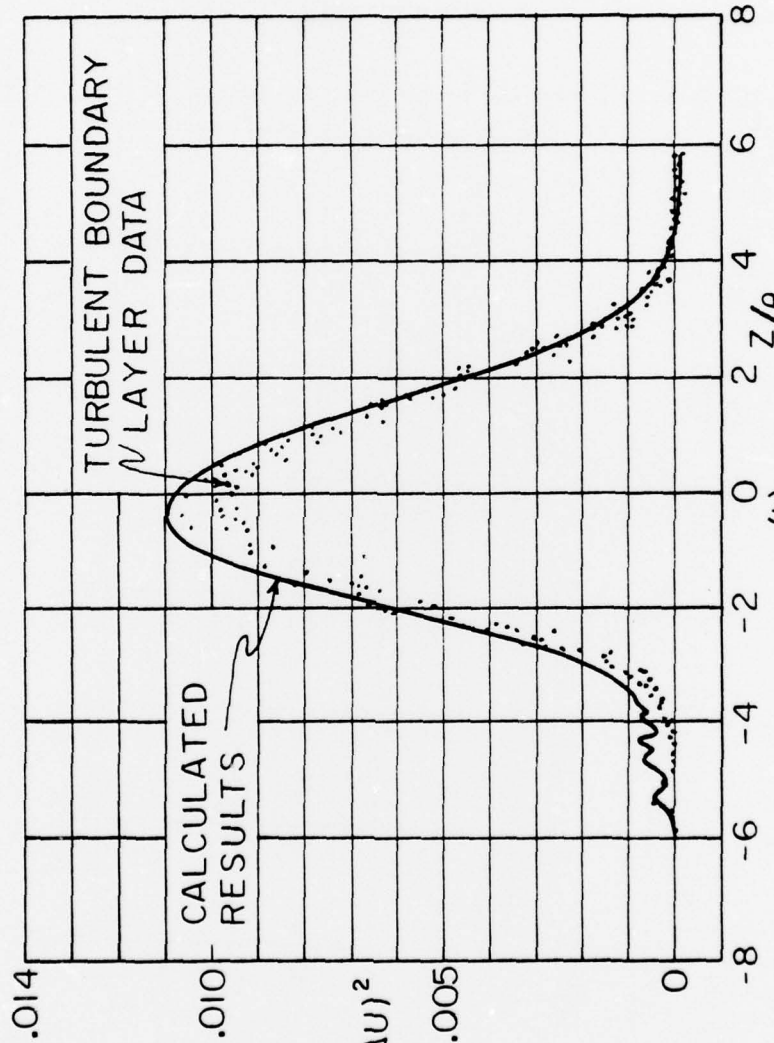

FIGURE 14. Comparison of computed and measured Reynolds stress distributions. (b) Turbulent boundary layer, $\lambda = .81$.

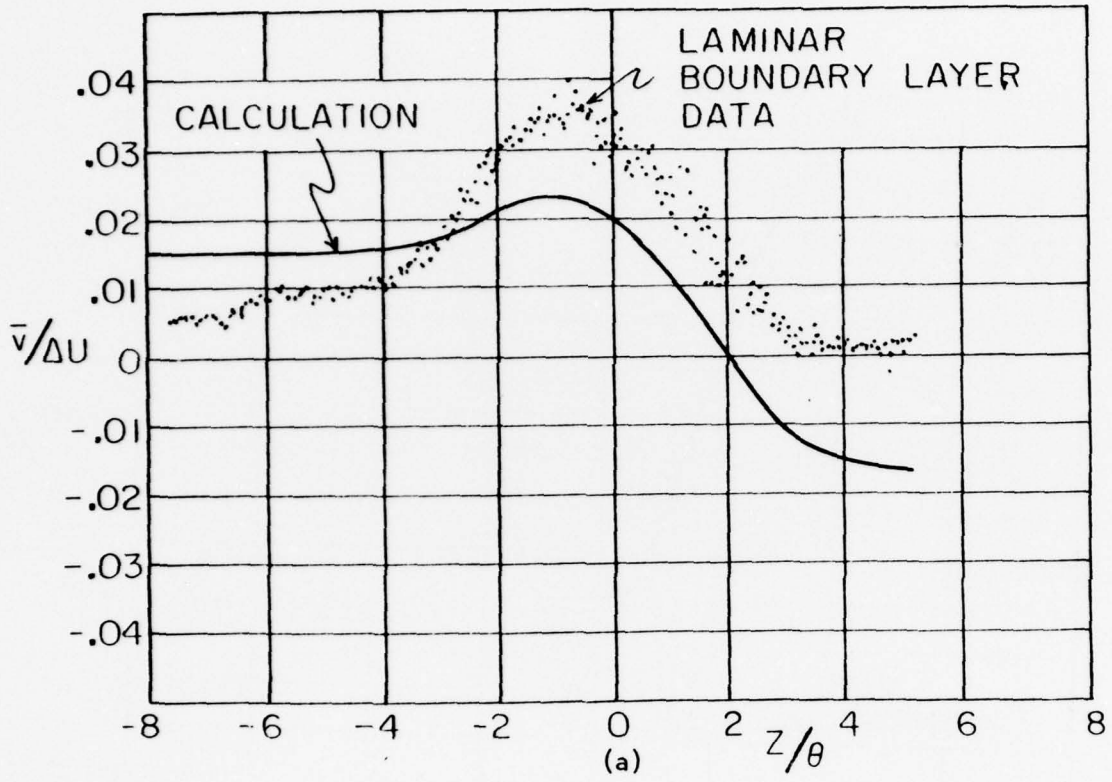

FIGURE 15. Comparison of computed and measured lateral mean velocity distributions. (a) Laminar boundary layer, λ =.82.

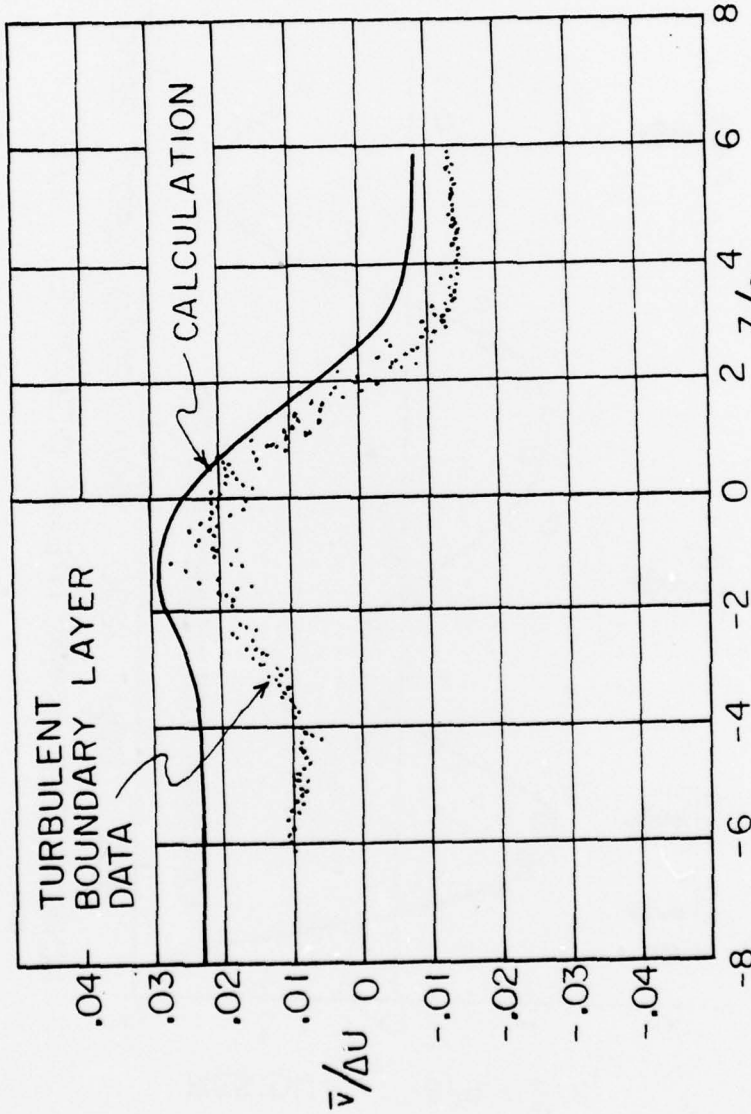

FIGURE 15. Comparison of computed and measured lateral mean velocity distributions. (b) Turbulent boundary layer, λ =.81.

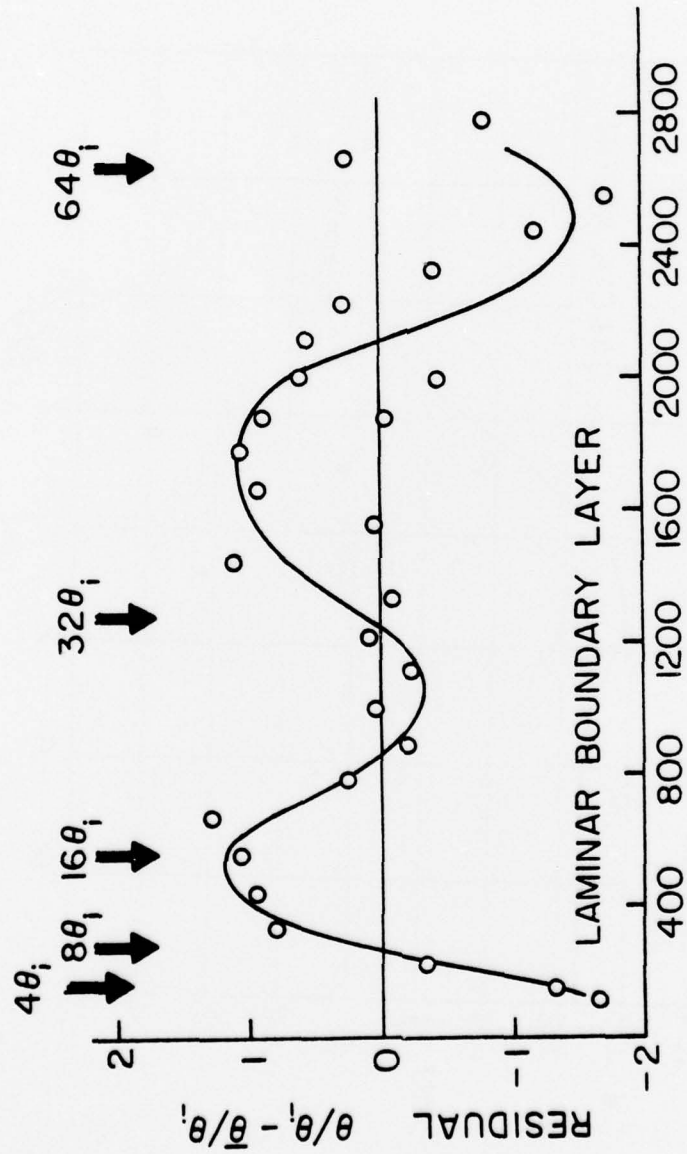

FIGURE 16. Residual momentum thickness (departure from best line) as a function of downstream distance for laminar boundary layer.

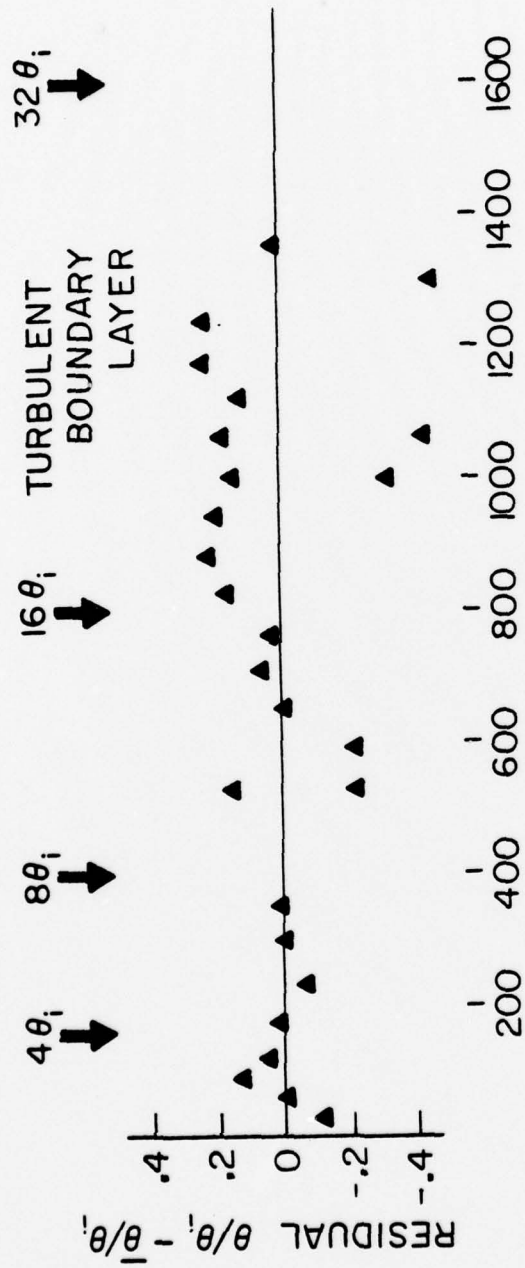

FIGURE 17. Residual momentum thickness versus downstream distance for turbulent boundary layer.

SECURITY CLASSIFICATION OF THIS PAGE (When Data Entered)

REPORT DOCUMENTATION PAGE		READ INSTRUCTIONS BEFORE COMPLETING FORM
1. REPORT NUMBER USC-1-PU	2. GOVT ACCESSION NO.	3. RECIPIENT'S CATALOG NUMBER
4. TITLE (and Subtitle) THE GROWTH OF THE TWO DIMENSIONAL MIXING LAYER FROM A TURBULENT AND NON TURBULENT BOUNDARY LAYER		5. TYPE OF REPORT & PERIOD COVERED Technical Report 6. PERFORMING ORG. REPORT NUMBER
7. AUTHOR(s) F. K. Browand and B. O. Latigo		8. CONTRACT OR GRANT NUMBER(s) N00014-75-C-1143 NR-098-038
9. PERFORMING ORGANIZATION NAME AND ADDRESS University of Southern California Los Angeles, California 90007		10. PROGRAM ELEMENT, PROJECT, TASK AREA & WORK UNIT NUMBERS
11. CONTROLLING OFFICE NAME AND ADDRESS Project SQUID Headquarters Chaffee Hall, Purdue University West Lafayette, Indiana 47907		12. REPORT DATE November 1978 13. NUMBER OF PAGES 35
14. MONITORING AGENCY NAME & ADDRESS(if different from Controlling Office) Office of Naval Research, Power Program, Code 473 Department of the Navy 800 No. Quincy Street Arlington, VA 22217		15. SECURITY CLASS. (of this report) Unclassified 15a. DECLASSIFICATION/DOWNGRADING SCHEDULE

16. DISTRIBUTION STATEMENT (of this Report)

This document has been approved for public release and sale; its distribution is unlimited.

17. DISTRIBUTION STATEMENT (of the abstract entered in Block 20, if different from Report)

Same

18. SUPPLEMENTARY NOTES

19. KEY WORDS (Continue on reverse side if necessary and identify by block number)

Mixing Layer

Turbulence

20. ABSTRACT (Continue on reverse side if necessary and identify by block number)

The effect of the initial boundary layer upon the downstream growth of the turbulent mixing layer between two streams is studied experimentally. Two streams is studied experimentally. Two conditions are carefully documented--in one case the boundary layers at separation are laminar; in the other case one boundary layer is made turbulent with a trip wire. When the boundary layer is turbulent, the lateral length scale, θ, characterizing the thickness of the mixing region, grows more slowly. At 400-500 initial momentum thicknesses

DD FORM 1 JAN 73 1473 EDITION OF 1 NOV 65 IS OBSOLETE
S/N 0102-LF-014-6601

Unclassified
SECURITY CLASSIFICATION OF THIS PAGE (When Data Entered)

theta

downstream, the growth rate relaxes toward--but does not meet--the growth rate of the untripped mixing layer. The lateral distributions of turbulence quantities, when scaled with the local lateral thickness, achieve the same form at distances beyond approximately 800 momentum thicknesses.